Available online at www.sciencedirect.com

ScienceDirect

Procedia Structural Integrity 7 (2017) 92–100

Structural Integrity Procedia

www.elsevier.com/locate/procedia

3rd International Symposium on Fatigue Design and Material Defects, FDMD 2017, 19-22 September 2017, Lecco, Italy

As-built surface layer characterization and fatigue behavior of DMLS Ti6Al4V

R. Konečná[a*], G. Nicoletto[b], S. Fintová[c], M. Frkáň[a]

[a]*Uuniversity of Zilina, Univerzitna 1,01026 Zilina, Slovakia*
[b]*University of Parma, Parco Area delle Scienze 181/A, Italy*
[c]*Institue of Physics of Materials, Zizkova 22, 61662 Czech Republic*

Abstract

Direct Metal Laser Sintering (DMLS) is a powder bed fusion technology used in the fabrication layer-by-layer of metallic parts directly from a CAD file. Since the fatigue behavior of DMLS Ti6Al4V is strongly influenced by the surface roughness of the as-built surface, fatigue tests were performed on smooth specimens produced with different orientations with respect to build using an EOS M 290 system. A SEM investigation and roughness measurements of the test surfaces were used to interpret the surface roughness as the contribution of i) roughness induced due to solidification of the melt pool (primary roughness); ii) roughness induced by partly melted powder particles (secondary roughness). Surface roughness modification from the as-built state by manual grinding was also investigated in fatigue and found to give a limited improvement. On the other hand, surface machining improves considerably the fatigue strength with respect to both the as-built condition and the manually ground condition.

Peer-review under responsibility of the Scientific Committee of the 3rd International Symposium on Fatigue Design and Material Defects.

Keywords: Ti6Al4V, direct metal laser sintering, heat treatments, fatigue, roughness, defects

* Corresponding author.
E-mail address: radomila.konecna@fstroj.uniza.sk

Peer-review under responsibility of the Scientific Committee of the 3rd International Symposium on Fatigue Design and Material Defects.
10.1016/j.prostr.2017.11.065

1. Introduction

The additive manufacturing technology, denominated Direct Metal Laser Sintering (DMLS), makes it possible to produce metallic components directly from a computer-aided design file of the part. DMLS involves a complex process where the material is fabricated layer-by-layer through a localized melting of gas atomized powder by a concentrated laser beam and its solidification, see Bandyopadhyay and Bose (2016).

Ti6Al4V is one of the most extensively used alloys for highly critical parts in aerospace and biomedical. The demanding reliability requirements of conventional Ti6Al4V parts are applied also to DMLS Ti6Al4V parts and require successfully passing fatigue validation by testing.

An important issue of the fatigue behavior of DMLS Ti6Al4V is the relatively high roughness, R_a up to 20 μm, of the as-built surface, see Edwards and Ramulu (2014), Bača et al. (2015), and Mower and Long (2016).

The roughness depends on a combination of raw material quality (powder particle size), additive manufacturing system and processing parameters, see Gong et al. (2013). Although machining may result in a smooth surface it is not always a viable approach from the economical and functional standpoints. As far as the role of surface quality on fatigue, Wycisk et al. (2014), reported an endurance limit of 210 MPa (R = 0.1, smooth geometry) for DMLS Ti6Al4V specimens with inherent surface roughness, a value significant lower compared to polished ones (greater than 500 MPa according to Mower and Long (2016)). These results were confirmed by Bača et al. (2016). The importance of surface roughness effect on fatigue motivates current studies on post processing methods. Alternatively, a fatigue damage model for an as-built DMLS surface may be identified and used to quantify the expected reduction factor as described in Greitemeier et al. (2015).

Besides AM process parameters and powder quality, as-built DMLS surfaces show different morphology in dependence of surface orientation with respect to the build direction. Fig. 1a shows the as-built top surface (perpendicular to build direction Z) with evidence of the raster pattern of the melt stripes. Fig. 1b shows an as-built lateral surface (i.e. planes X-Z or Y-Z) with a grainy surface due to partly melted powder grains superposed to the smooth melted material. A section of the top as-built surface shown in Fig. 1c highlights a low roughness with local shallow notches between neighboring melt strips. The section of a lateral surface, shown in Fig. 1d, is rather different with notches between fully melt layers but also a system partly melted powder particles attached to the surface.

a) 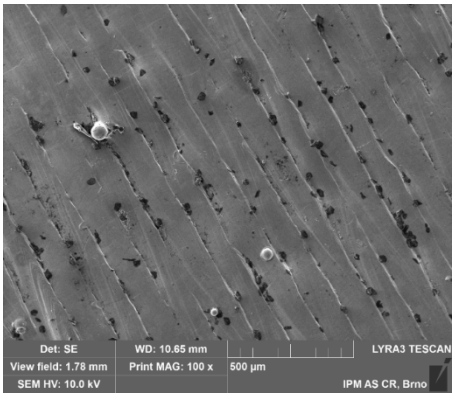

b) 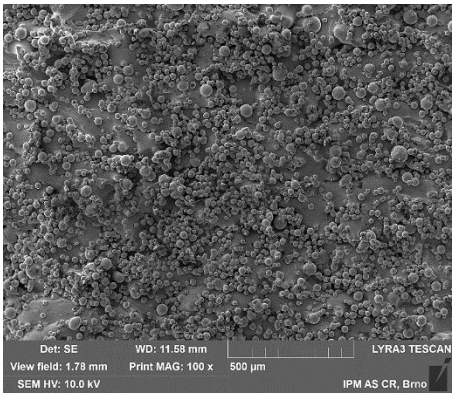

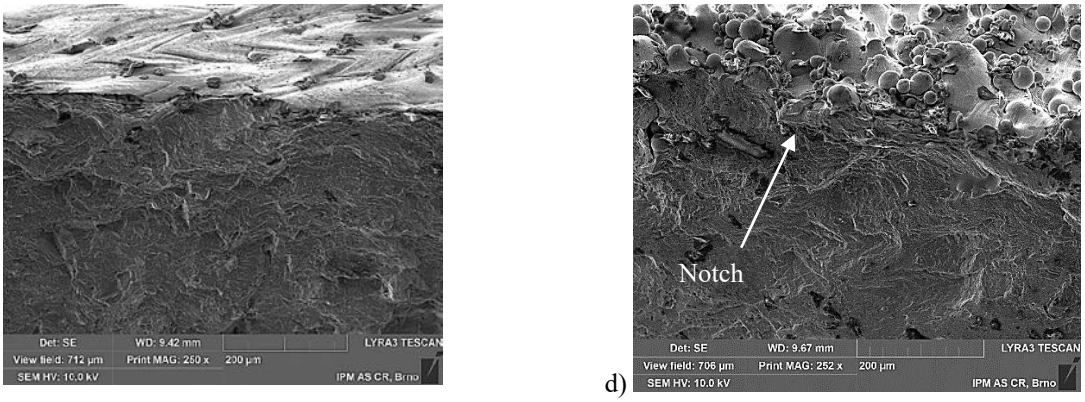

c) d)

Fig. 1 a) as-built surface perpendicular to build direction, b) as-built surface parallel to build direction, c) profile of as-built surface of Fig. 1a and d) profile of as-built surface of Fig. 1b, SEM.

Fig. 1 shows how surface roughness measurements of as-built surfaces will combine in a single parameter the influence of the partly melted particles and of the melted layers but will not account for the presence of notches (surface and subsurface) that are expected to affect the fatigue behavior via early crack initiation.

The present authors are interested in investigating whether such roughness measurements of as-built surfaces are representative of the associated fatigue strength. Therefore, fatigue test results performed on smooth specimens produced with different orientations with respect to build and with either as-built or manually polished surfaces are compared to surface roughness characterization and measurements.

2. Experimental details

2.1. Material and specimen fabrication

The issue of as-built surface roughness and fatigue behavior is investigated using directional fatigue specimens of DMLS Ti6Al4V with as-built surfaces. Miniature fatigue plane bending specimens, proposed by Nicoletto (2016), were produced so that the applied cyclic stress was directed in three different orientations with respect to build direction.

The DMLS process used Ti6Al4V ELI alloy powder supplied by EOS GmbH with spherical powder particles and a predominant diameter range from 25 to 45 µm. The fatigue specimens were fabricated using an EOS M 290 system. This system uses an Yb fiber laser unit with a wavelength of 1075 nm with a max laser power of 400 W and layer thickness of 60 µm. The selective laser melting process took place under protective argon atmosphere with a process chamber temperature of 80 °C. The laser scanning strategy is based on a shell and core concept whereby the contour of the layer is first melted then the internal part of the layer is melted by raster laser motion, clearly visible in Fig. 1a. The raster scanning of successive layers is performed after rotation of a specified angle.

While the motivation behind the special specimen geometry is discussed by Nicoletto (2016), Fig. 2 schematically shows the positioning on the build plate of individual specimens with three different orientations with respect to the build direction and the respective denomination. It is noted that the surface under investigation is the flat surface opposite to the semicircular notch. Fatigue testing is performed under a cyclic tensile loading with $R = 0$ using a plane bending test machine. The stress orientation is different for the three specimens of Fig. 2: namely the top layer of the fabrication phase (see Fig. 1a) is tested in specimen A, the applied stress direction is perpendicular to the transformed layers in specimen C while the stress is parallel to the layers in specimen B. Type B and Type C specimens have surfaces under test such as Fig. 1b.

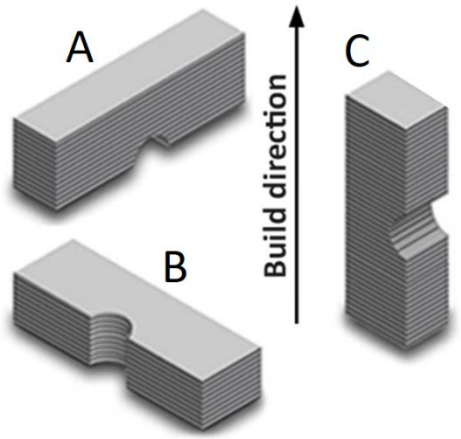

Fig. 2 Directional fabrication of fatigue specimens and denomination.

Fig. 3 As-built (left) and manual ground (right) surfaces of Type A specimens.

After fabrication and removal from build plate, all mini specimens were heat treated in a vacuum furnace as follows: 740 °C for 2 h then slow cooling in vacuum to 530 °C and final cooling to room temperature in Argon atmosphere. This heat treatment reduces residual stresses of the fabrication process to negligible levels. Tensile testing on smooth specimens provided the following characteristics: tensile strength R_m= 1176 MPa, yield stress $R_{p0.2}$ = 1104 MPa and elongation to rupture A = 12.9 %.

Besides fatigue tests of directional heat treated specimens with as-built surfaces, several specimens were tested after manual grinding of the surface under load. The manual dry grinding process was performed using two SiC abrasive papers: initially a rough (grit size 500) paper and then a fine (grit size 1000) paper. This manual grinding is expected to remove only part of the roughness, while typically surface machining would remove a thicker surface layer (> 200 μm). Fig. 3 shows a Type A specimen in the as-built state and after manual grinding.

2.2. Material characterization

The microstructure was observed using a light optical microscope Zeiss Axio Observer Z1M on polished and etched (10% HF for 10 s) samples that were cut from the fatigue testing specimens. The microstructure consists of fine needles of α-phase in β matrix, see Konečná (2017).

Surface roughness of the as-built surfaces was measured in the longitudinal direction on the loading plane subjected to cyclic tensile loading on a Mitutoyo SJ 210 machine. The achieved roughness of the manually ground specimens was also quantified. An Olympus LEXT OLS3100 confocal microscope with AFM module was also used to map the as built surface roughness.

After fatigue fracture surfaces and fracture profiles were examined in a SEM Tescan LYRA 3 XMU FEG/SEM.

2.3. Fatigue testing

Fatigue experiments were performed under cyclic plane bending on a Schenk type testing machine modified to continuous monitoring of the applied load during the test under a constant displacement range. The apparatus applied cyclic tensile stress (R = 0) to the flat as-built specimen face at a frequency of 15 Hz. Test were interrupted above 2 x 10^6 cycles, if specimen did not fail (i.e. run-out).

3. Results and discussion

3.1. Surface characterization

The results of the roughness measurements Ra and Rz of the different surface specimens in the as-built state are shown in Tab. 1. Considering the different origin of the as-built top and lateral surfaces demonstrated in Fig 1, interestingly but not unexpectedly, significant differences are determined: namely type C and B specimens show the highest roughness, and Type A specimens the lowest. Fig. 1a shows what can now be defined primary roughness as it is due to the melted layers and stripes. This primary roughness measurement of Type A specimen is shown in Tab. 1. Fig. 1b shows that the roughness is due to the superposition of the primary and the secondary roughness due to partially melted particles which results in the higher roughness in Table 1 for Type B and C specimens. So the secondary roughness contributes Ra = 10 μm of the total roughness Ra = 13 μm.

In Geitemeier et al. (2015) it is reported that the orientation of part in the build chamber has a large impact on the roughness with the surface roughness of a surface parallel to the vertical build direction, Z, that can be 2-3 times rougher than a flat horizontal surface. Here it is even 4 times rougher.

Table 1 Surface roughness of the plane under fatigue loading

Roughness	Type A	Type B	Type C	A and C after grinding
Ra [μm]	3.3 ± 0	13.1 ± 0.3	13.4 ± 0.5	0.19 ± 0.03
Rz [μm]	20.1 ± 3.3	88.8 ± 8.7	80.7 ± 8.2	1.52 ± 0.15

The confocal microscope images of Fig. 4 show clearly that the top layer of Type A specimen is characterized by a regular and well defined pattern of solidified raster tracks with limited powder entrapment (i.e. primary roughness), while the lateral surface shows a grainy appearance of partially melted powder particles. The width and depth of the coarse pattern of Fig. 4a is correlated to the size (depth and width) of the melt pool, which depends on the layer thickness (i.e. 60 μm).

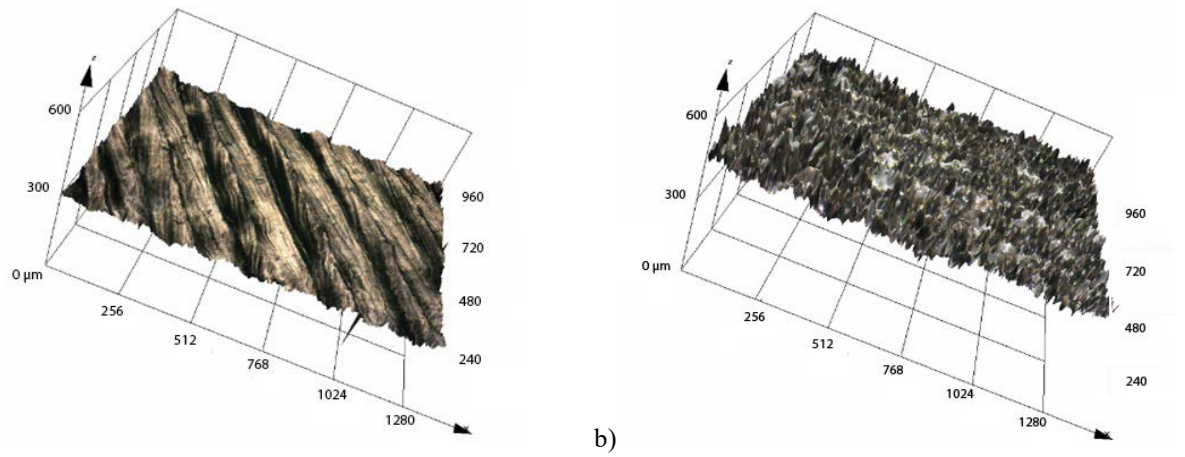

a) b)

Fig. 4 Confocal microscopic evaluation of as-built surface of Type A, a) top surface and b) lateral surface.

3.2. Directional effect of as-built surfaces on fatigue behavior

Fatigue test results of directional as-built Type A and Type C mini-specimens of DMLS Ti6Al4V are shown in Fig. 5. Differently from previous results on DMLS Ti6Al4V by Bača et al. (2016), where type C specimens showed a significantly lower fatigue strength compared to the other two directions, the present heat treatment in vacuum

results in rather similar high cycle fatigue data trends with a shift for specimen type C to shorter lives. Each specimen type shows limited scatter. It is stressed also that differently from other literature data obtained at under the same load ratio R = 0 or 0.1, here the data are presented in terms of stress amplitude σ_a rather than maximum stress σ_{max}. The present data are coherent with the results of Nicoletto (2016) and Mower and Long (2016) on the same DMLS alloy.

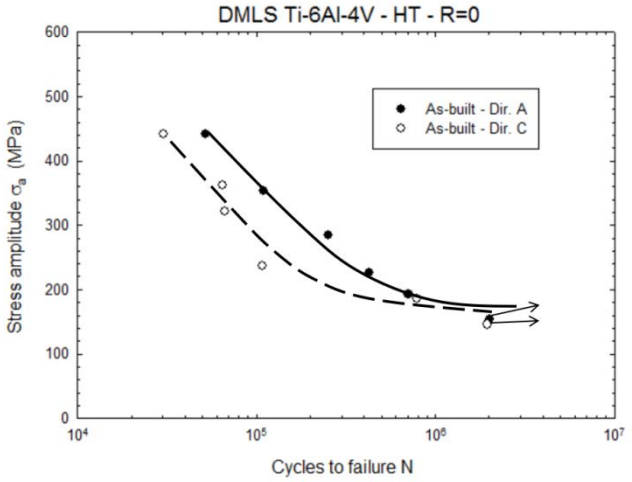

Fig. 5 Fatigue curves of as-built and heat treated specimens of Ti6Al4V.

3.3. Effect of ground and machined surfaces on fatigue behavior

The influence of the manual grinding of the flat surface on the fatigue behavior for two specimen directions (i.e. A and C of Fig. 2) are shown in Fig. 6 and 7. The manual grinding of the top surface does not significantly affect the fatigue behavior of Type A specimens when compared to the fatigue response in the as-built state. A possible benefit at long lives may be inferred by the however limited data.

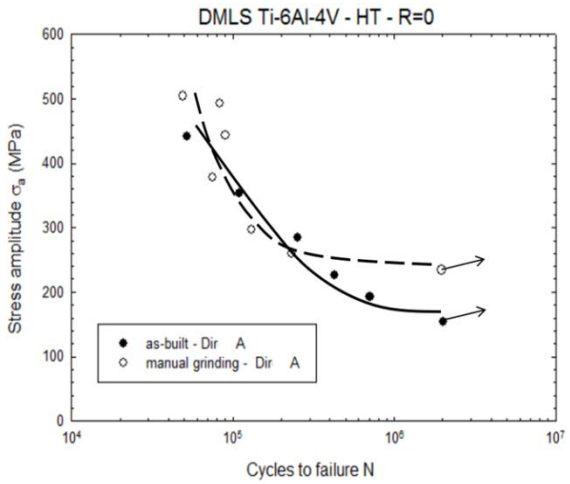

Fig. 6 Fatigue curves of Type A specimens in as-built and manual ground conditions.

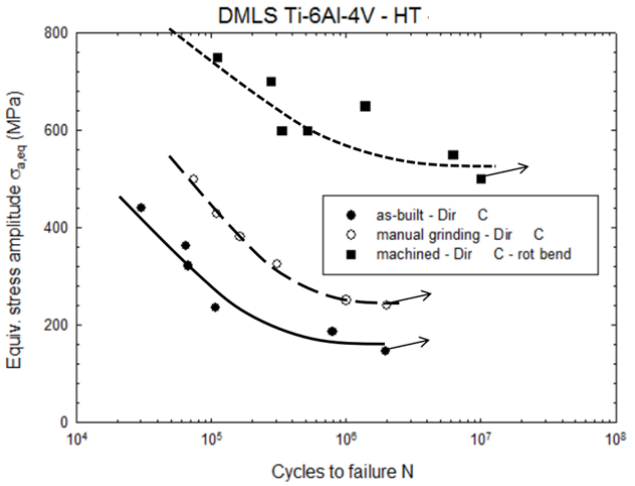

Fig. 7 Fatigue curves of Type C specimens in as-built and in manually ground conditions (R = -1). Rotating bending test results of machined specimens are also included.

To place the present results in a broader perspective, original rotating bending fatigue tests results (stress amplitude σ_a at R = -1) on the same heat treated DMSL Ti6Al4V material after machining of the surface are also considered. Since the rotating bending specimens were produced with the axis parallel to the build direction, therefore oriented as Type C mini specimens, they are introduced in Fig. 7 along with the Type C specimen results.

To do so, a conversion of the R = 0 fatigue test data obtained with the mini specimens under plane bending loading into an equivalent stress amplitude $\sigma_{a,eq}$ at R = -1 is preliminarily performed using the Haigh relation of the mean stress effect on fatigue, see Juvinall and Marshek (2012). When R = 0, that is when stress amplitude σ_a is equal to the mean stress σ_m the Haigh relation is the following

$$\sigma_{a,eq}=\sigma_a\,(R_m/(R_m-\sigma_a)) \tag{1}$$

where σ_a is the stress amplitude of the fatigue test at R = 0 and R_m is the tensile strength of DMSL Ti6Al4V. Inspection of Fig. 7 shows that manual grinding has a significant effect on fatigue in the case of Type C specimens where the fatigue curves in Fig. 7 are separated by a sizable and uniform increment of about 60 % of the manually ground surface data with respect to the as-built surface data. Fig. 7 shows also that surface machining results in considerably higher fatigue strength compared to manual grinding.

Therefore, the surface roughness of the as-built DMLS Ti6Al4V with the morphology shown in Fig. 1 and measured in Table 1 is only partially descriptive of the fatigue behavior. Manual grinding of Type C mini specimens to a considerably lower surface roughness, see Table 1, improves their fatigue response, but not to the degree associated to a machining operation, which removes a surface layer of significant depth.

3.4. Fatigue fracture surfaces

Typical fatigue fracture surfaces of mini specimens were investigated in the SEM and are shown in Fig. 8a and 8b for Type A and Type C specimens, respectively. Their fracture profiles (intersection of surface under load and fracture surface) and initiation places are shown in Fig. 8c and 8d. Typically Type A specimens showed only one initiation place of fatigue fracture located in the corner with the coarser lateral side, Fig. 8c, with the presence of many micro shrinkages that acted as initiation places, (see white arrows in Fig. 8c).

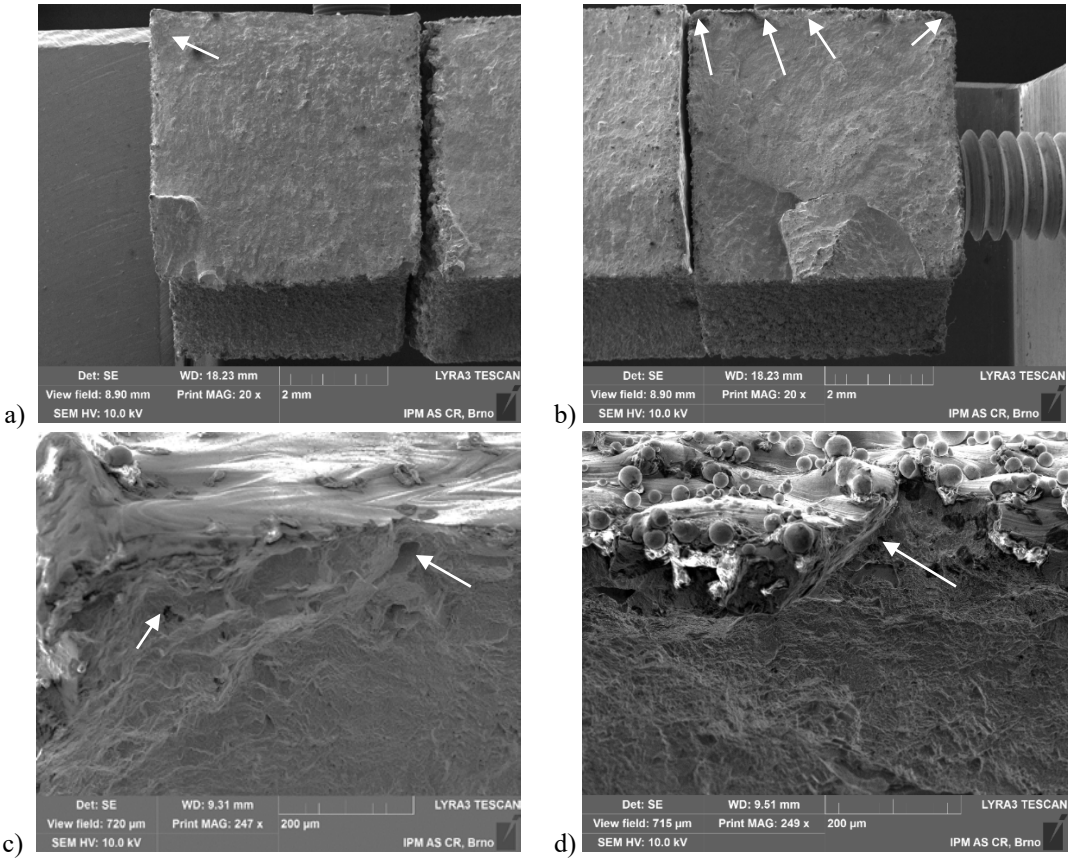

Fig. 8 Fatigue fracture surfaces of as-built specimens a) orientation A, b) orientation C and initiation places c) one initiation place for A and multiple initiation places for C, SEM.

The fracture profile of Type C specimens is characterized by high surface roughness (Table 1) and multiple initiation places (white arrow) at notches associated to the primary roughness due to the sequence of melted layers, see Fig. 8d. Crack initiation did not occur at internal defects.

Therefore, the fatigue strength of as-built Type C specimens is influenced by the roughness of the plane under loading which is a combination of a primary roughness (layer thickness dependent) and a secondary roughness (partly melted particles dependent). Elimination of the secondary roughness (by manual grinding) improves the fatigue strength but not to the degree of a machining operation. The fatigue strength of as-built Type A specimens is not significantly better than the Type C even if the surface layer has a lower roughness (limited secondary roughness) because crack initiation occurs at corners with rougher surfaces. These observations explain the fatigue results of Fig. 5, Fig. 6 and Fig. 7.

4. Conclusions

Fatigue test results were performed on smooth specimens of heat treated DMSL Ti6Al4V produced with different orientations with respect to build. Surface roughness characterization and measurements of as-built or manually ground flat surfaces have been performed and compared to test results. The following conclusions are reached:

- As-built surfaces show a slight directional effect on fatigue behavior.
- The as-built roughness is the combination of a primary roughness related to the process parameters and a secondary roughness due to the partially melted and entrapped powder particles.
- Removal of the surface roughness by manual grinding improves the fatigue strength of Type C specimens with respect to the as-built condition.

- Surface machining improves considerably the fatigue strength with respect to both the as-built condition and the manually ground condition.

Acknowledgements

The research was supported by the project Slovak VEGA grant No. 1/0685/2015. Specimen production by partner company BEAM-IT srl, Fornovo Taro, Italy is acknowledged with thanks.

References

Bača, A., Konečná, R., Nicoletto, G., Kunz, L., 2015. Effect of surface roughness on the fatigue life of laser additive manufactured Ti6Al4V alloy. Manufacturing technology, 15 (4), 498-502.

Bača, A., Konečná, R., Nicoletto, G., Kunz, L., 2016. Influence of build direction on the fatigue behaviour of Ti6Al4V alloy produced by direct metal laser sintering. Materials Today: Proceedings 3, 921-924.

Bača, A., Konečná, R., Nicoletto, G., 2017. Influence of the direct metal laser sintering process on the fatigue behavior of the Ti6Al4V alloy. Materials Science Forum, Vol. 891, 317-321.

Bandyopadhyay, A., Bose, A., 2016. Additive manufacturing: Additive manufacturing technologies of metals using powder-based technology. Taylor & Francis Group: Boca Raton, 377.

Edwards, P., Ramulu, M., 2014. Fatigue performance evaluation of selective laser melted Ti–6Al–4V. Mater. Sci. Eng. A, A598, 327–337.

Gong, H., Rafi, K., Starr, T., Stucker, B., 2013. The effects of processing parameters on defect regularity in Ti-6Al-4V parts fabricated by selective laser melting and electron beam melting, 24th Annual International Solid Freeform Fabrication Symposium, 424-439.

Greitemeier, D., Dalle Donne, C., Syassen, F., Eufinger, J., Melz, T., 2015. Effect of surface roughness on fatigue performance of additive manufactured Ti–6Al–4V. Materials Science and Technology, 629-634.

Juvinall, R., Marshek, K.M., 2012. Fundamentals of Machine Component Design, New York: John Wiley, 929.

Konečná, R., Nicoletto. G., Bača, A., Kunz, L., 2017. Metallographic characterization and fatigue damage initiation in Ti6Al4V alloy produced by direct metal laser sintering. Materials Science Forum, Vol. 891, 311-316.

Mower, T. M., Long, M. J., 2016. Mechanical behavior of additive manufactured, powder-bed laser-fused materials. Materials Science and Engineering, A651 198-213.

Nicoletto, G., 2016. Anisotropic high cycle fatigue behavior of Ti-6Al-4V obtained by powder bed laser fusion. International Journal of Fatigue, vol. 94, 255-262.

Wycisk, E., Solbach, A., Siddique, S., Herzog, D., Walther, F., Emmelmann, C, 2014. Effects of defects in laser additive manufactured Ti–6Al–4V on fatigue properties. Phys. Proc, 56, 371–378.